Mineralogical Magazine, October 2016, Vol. 80(6), pp. 1055–1065

Lead-tellurium oxysalts from Otto Mountain near Baker, California, USA: XII. Andychristyite, $PbCu^{2+}Te^{6+}O_5(H_2O)$, a new mineral with *hcp* stair-step layers

ANTHONY R. KAMPF[1,*], MARK A. COOPER[2], STUART J. MILLS[3], ROBERT M. HOUSLEY[4] AND GEORGE R. ROSSMAN[4]

[1] Mineral Sciences Department, Natural History Museum of Los Angeles County, 900 Exposition Blvd., Los Angeles, CA 90007, USA
[2] Department of Geological Sciences, University of Manitoba, Winnipeg, Manitoba, R3T 2N2, Canada
[3] Geosciences, Museum Victoria, GPO Box 666, Melbourne 3001, Victoria, Australia
[4] Division of Geological and Planetary Sciences, California Institute of Technology, Pasadena, CA 91125, USA

[*Received 10 September 2015; Accepted 15 October 2015; Associate Editor: G. Diego Gatta*]

ABSTRACT

Andychristyite, $PbCu^{2+}Te^{6+}O_5(H_2O)$, is a new tellurate mineral from Otto Mountain near Baker, California, USA. It occurs in vugs in quartz in association with timroseite. It is interpreted as having formed from the partial oxidation of primary sulfides and tellurides during or following brecciation of quartz veins. Andychristyite is triclinic, space group $P\bar{1}$, with unit-cell dimensions $a = 5.322(3)$, $b = 7.098(4)$, $c = 7.511(4)$ Å, $\alpha = 83.486(7)$, $\beta = 76.279(5)$, $\gamma = 70.742(5)°$, $V = 260.0(2)$ Å^3 and $Z = 2$. It forms as small tabular crystals up to ~50 μm across, in sub-parallel aggregates. The colour is bluish green and the streak is very pale bluish green. Crystals are transparent with adamantine lustre. The Mohs hardness is estimated at between 2 and 3. Andychristyite is brittle with an irregular fracture and one perfect cleavage on {001}. The calculated density based on the empirical formula is 6.304 g/cm^3. The mineral is optically biaxial, with large 2V, strong dispersion, and moderate very pale blue-green to medium blue-green pleochroism. The electron microprobe analyses (average of five) provided: PbO 43.21, CuO 15.38, TeO_3 35.29, H_2O 3.49 (structure), total 97.37 wt.%. The empirical formula (based on 6 O apfu) is: $Pb_{0.98}Cu^{2+}_{0.98}Te^{6+}_{1.02}O_6H_{1.96}$. The Raman spectrum exhibits prominent features consistent with the mineral being a tellurate, as well as an OH stretching feature confirming a hydrous component. The eight strongest powder X-ray diffraction lines are [d_{obs} in Å(*I*)(*hkl*)]: 6.71(16)(010), 4.76(17)(110), 3.274(100)(120,102,012), 2.641(27)($\bar{1}$02, 211, $\bar{1}\bar{1}$2), 2.434(23)(multiple), 1.6736(17)(multiple), 1.5882(21)(multiple) and 1.5133(15)(multiple). The crystal structure of andychristyite ($R_1 = 0.0165$ for 1511 reflections with $F_o > 4\sigma F$) consists of stair-step-like *hcp* polyhedral layers of $Te^{6+}O_6$ and $Cu^{2+}O_6$ octahedra parallel to {001}, which are linked in the [001] direction by bonds to interlayer Pb atoms. The structures of eckhardite, bairdite, timroseite and paratimroseite also contain stair-step-like *hcp* polyhedral layers.

KEYWORDS: andychristyite, new mineral, tellurate, crystal structure, Raman spectroscopy, *hcp* layers, eckhardite, Otto Mountain, California.

Introduction

ANDYCHRISTYITE is the 14th new mineral to be described from the remarkable Pb-Cu-Te-rich secondary mineral assemblage at Otto Mountain, near Baker, California, USA (Kampf *et al.*, 2010*a*; Housley *et al.*, 2011). The other minerals first described from here (in order of description) are ottoite, $Pb_2Te^{6+}O_5$ (Kampf *et al.*, 2010*a*), housleyite, $Pb_6Cu^{2+}Te^{6+}_4O_{18}(OH)_2$ (Kampf *et al.*, 2010*b*), thorneite, $Pb_6(Te^{6+}_2O_{10})(CO_3)Cl_2(H_2O)$ (Kampf *et al.*, 2010*c*), markcooperite, $Pb_2(UO_2)Te^{6+}O_6$ (Kampf

* E-mail: akampf@nhm.org
DOI: 10.1180/minmag.2016.080.042

et al., 2010*d*), timroseite, $Pb_2Cu_5^{2+}(Te^{6+}O_6)_2(OH)_2$ (Kampf *et al.*, 2010*e*), paratimroseite, $Pb_2Cu_4^{2+}(Te^{6+}O_6)_2(H_2O)_2$ (Kampf *et al.*, 2010*e*), telluroperite, $Pb_3Te^{4+}O_4Cl_2$ (Kampf *et al.*, 2010*f*), chromschieffelinite, $Pb_{10}Te_6^{6+}O_{20}(OH)_{14}(CrO_4)(H_2O)_5$ (Kampf *et al.*, 2012), fuettererite, $Pb_3Cu_6^{2+}Te^{6+}O_6(OH)_7Cl_5$ (Kampf *et al.*, 2013*a*), agaite, $Pb_3Cu^{2+}Te^{6+}O_5(OH)_2(CO_3)$ (Kampf *et al.*, 2013*b*), bairdite, $Pb_2Cu_4^{2+}Te_2^{6+}O_{10}(OH)_2(SO_4)\cdot H_2O$ (Kampf *et al.*, 2013*c*), eckhardite, $(Ca,Pb)Cu^{2+}Te^{6+}O_5(H_2O)$ (Kampf *et al.*, 2013*d*) and mojaveite, $Cu_6[Te^{6+}O_4(OH)_2](OH)_7Cl$ (Mills *et al.*, 2014). It is noteworthy that all of these contain essential Te, all but two contain essential Pb, and all but four contain essential Cu.

The mineral is named for Andrew (Andy) Gregor Christy (b. 1963), a Welsh–Australian mineralogist, petrologist, geochemist and solid-state chemist, for his contributions to mineralogy and, in particular, for the descriptions of new minerals (kapundaite, mössbauerite, mojaveite, bluebellite and favreauite), his work on minerals of the sapphirine supergroup (e.g. Christy *et al.*, 2002; Christy and Grew, 2004), pyrochlore supergroup (e.g. Atencio *et al.*, 2010) and hydrotalcite supergroup (e.g. Mills *et al.*, 2012), and more recently for helping advance the knowledge of the crystal chemistry of tellurium (e.g. Mills and Christy, 2013; Christy and Mills, 2013; Christy *et al.*, 2016). Andy Christy has agreed to the naming of this mineral in his honour. Note that the compound name 'andychristyite' is proposed instead of the simpler 'christyite' because of the similarity of the latter to the existing mineral names christite and christelite.

The new mineral and name have been approved by the Commission on New Minerals, Nomenclature and Classification of the International Mineralogical Association (IMA2015–024). The holotype specimen is deposited in the Natural History Museum of Los Angeles County under catalogue number 65577.

Occurrence

Andychristyite was found on the small dump outside the entrance to the Aga mine (35.27215°N, 116.09487°W, elevation 1055 feet) on Otto Mountain, 1 mile northwest of Baker, San Bernardino County, California.

Andychristyite is extremely rare and has only been found as a few crystals in a single small vug in quartz. The holotype specimen was collected by Eckhard D. Stuart. The only other phase in the vug was identified visually as timroseite. Elsewhere on the specimen are found goethite and hematite, and bright green inclusions of what appears to be khinite are seen in the quartz matrix in close proximity to the vug. Other species identified in the mineral assemblages at Otto Mountain include acanthite, agaite, anglesite, anatacamite, atacamite, bairdite, boleite, brochantite, burckhardtite, calcite, caledonite, celestine, cerussite, chalcopyrite, Br-rich chlorargyrite, chromschieffelinite, chrysocolla, devilline, diaboleite, eckhardite, eztlite, fluorite, fornacite, frankhawthorneite, fuettererite, galena, gold, hessite, housleyite, iodargyrite, jarosite, kenyaite, kuranakhite, linarite, malachite, markcooperite, mattheddleite, mcalpineite, mimetite, mojaveite, mottramite, munakataite, murdochite, muscovite, ottoite, paratimroseite, perite, phosphohedyphane, plumbojarosite, plumbotsumite, pyrite, telluroperite, thorneite, vanadinite, vauquelinite, wulfenite and xocomecatlite.

Andychristyite is a secondary oxidation-zone mineral and is presumed to have formed by oxidation of earlier formed tellurides, chalcopyrite and galena. Additional background on the occurrence is provided in Kampf *et al.* (2010*a*), Housley *et al.* (2011) and Christy *et al.* (2016).

Physical and optical properties

Andychristyite occurs as bluish-green tablets flattened on {001}, up to ~50 μm across (Fig. 1). Only the {001} form was observed; the crystals were too small and imperfectly formed to determine other crystal forms. No twinning was observed optically under crossed polars or based upon single-crystal X-ray diffraction. The streak is very pale bluish green. Crystals are transparent with adamantine lustre. Andychristyite does not fluoresce under longwave or shortwave ultraviolet light. The Mohs hardness could not be measured, but is estimated to be between 2 and 3, based upon the behaviour of crystals when broken. The mineral is brittle with irregular fracture. Cleavage is perfect on {001}. The density could not be measured because it is greater than those of available high-density liquids and there is insufficient material for physical measurement. The calculated density based on the empirical formula and single-crystal cell is 6.304 g/cm^3. Andychristyite crystals decompose rapidly in dilute HCl at room temperature.

The Gladstone–Dale relationship (Mandarino, 2007) predicts an average index of refraction of 2.011. The unavailability of index liquids with $n > 2$

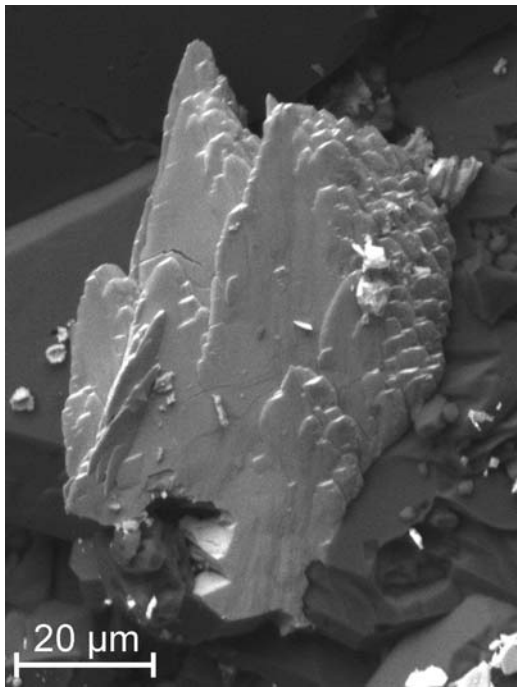

FIG. 1. Back-scatter scanning electron microscopy image of andychristyite on quartz.

precluded the measurement of the mineral's indexes of refraction. This fact, as well as the very small crystal size and very limited amount of material, made the determination of most optical properties impractical. One optic axis is oriented almost perpendicular to {001}, allowing limited conoscopic observation. The mineral is optically biaxial with undetermined sign. The 2V is large and the dispersion is strong, but the sense could not be determined. Pleochroism is moderate, varying from very pale blue-green to medium blue-green.

Raman spectroscopy

Raman spectroscopic microanalyses were carried out using a Renishaw M1000 micro-Raman spectrometer system. Light from a 514.5 nm solid-state laser was focused onto the sample with a 100 × objective lens. At 10% laser power the system provides ~5 mW of power at the sample, in a spot size of ~1 µm. Peak positions were calibrated against a silicon (520.5 cm^{-1}) standard. All spectra were obtained with a dual-wedge polarization scrambler inserted directly above the objective lens to minimize the effects of polarization.

The sample used for the Raman spectra was the polished microprobe sample, which contains several grains of andychristyite. The dominant features of the spectrum (Fig. 2) are bands at 708, 665 and 625 cm^{-1}. Tellurates have been shown previously to have the components of their ν_1 band in the 600 to 800 cm^{-1} region (Blasse and Hordijk, 1972; Frost, 2009; Frost and Keeffe, 2009; Kampf *et al.*, 2013*c*). Also noteworthy is an OH stretching feature centred around 3306 cm^{-1} that is an

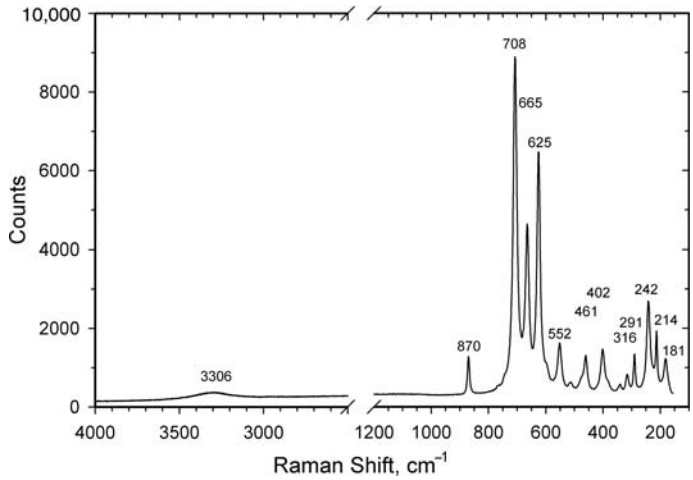

FIG. 2. The Raman spectrum of andychristyite that shows multiple features in the tellurate region with the two strongest lines at 708 and 625 cm^{-1}.

TABLE 1. Powder X-ray diffraction data for andychristyite.

I_{obs}	d_{obs}	d_{calc}	I_{calc}	$h\ k\ l$	I_{obs}	d_{obs}	d_{calc}	I_{calc}	$h\ k\ l$	I_{obs}	d_{obs}	d_{calc}	I_{calc}	$h\ k\ l$
11	7.36	7.2913	10	0 0 1	2	2.0185	2.0142	2	$\bar{1}$ 0 3			1.5449	1	$\bar{2}$ $\bar{4}$ 1
16	6.71	6.6959	28	0 1 0	5	1.9689	1.9715	4	2 $\bar{1}$ 2	4	1.5403	1.5439	2	0 4 2
4	5.03	5.0289	4	0 1 1			1.9549	2	$\bar{1}$ 2 2			1.5336	1	$\bar{1}$ 1 4
7	4.90	4.9089	4	1 0 0			1.9467	1	2 0 3			1.5268	2	$\bar{2}$ $\bar{2}$ 3
		4.8401	6	0 $\bar{1}$ 1	11	1.9346	1.9343	6	2 2 3			1.5165	3	1 $\bar{2}$ 4
17	4.76	4.7295	14	1 1 0			1.9334	3	$\bar{2}$ 1 1			1.5150	2	3 0 3
6	4.47	4.4703	5	1 1 1			1.9233	1	2 3 2	15	1.5133	1.5133	3	1 4 3
10	3.723	3.7214	10	$\bar{1}$ 0 1			1.8792	3	$\bar{1}$ 1 3			1.5114	4	3 $\bar{1}$ 1
6	3.622	3.6040	9	$\bar{1}$ $\bar{1}$ 1	4	1.8739	1.8718	3	0 $\bar{3}$ 2			1.5094	1	2 $\bar{2}$ 3
12	3.477	3.4732	19	$\bar{1}$ 1 0			1.8513	4	1 1 4			1.4996	1	0 $\bar{4}$ 2
		3.3479	1	0 2 0	7	1.8362	1.8416	1	1 0 4			1.4947	1	1 1 5
		3.3081	8	1 $\bar{1}$ 1			1.8273	4	$\bar{2}$ $\bar{3}$ 1	2	1.4643	1.4705	2	$\bar{2}$ 1 3
		3.2876	29	1 2 0	7	1.8136	1.8228	3	0 0 4			1.4583	1	0 0 5
100	3.274	3.2803	33	1 0 2			1.8049	5	$\bar{1}$ $\bar{2}$ 3			1.4513	1	$\bar{1}$ 4 0
		3.2547	38	0 1 2			1.7927	1	1 $\bar{3}$ 1			1.4414	2	$\bar{2}$ 3 0
		3.2227	4	1 2 1			1.7905	1	1 $\bar{2}$ 3			1.4391	2	0 3 4
		3.1514	7	0 $\bar{1}$ 2			1.7762	1	0 1 4	7	1.4366	1.4364	1	0 1 5
		3.0878	1	0 2 1			1.7459	1	3 2 1			1.4280	1	$\bar{1}$ 3 3
3	3.006	2.9992	6	0 $\bar{2}$ 1			1.7432	1	2 $\bar{1}$ 3			1.4235	1	2 1 5
6	2.795	2.8129	5	$\bar{1}$ $\bar{2}$ 1			1.7419	4	0 $\bar{1}$ 4			1.4121	1	1 $\bar{1}$ 5
9	2.698	2.6970	10	1 $\bar{1}$ 2	11	1.7365	1.7366	2	$\bar{2}$ 2 0			1.4105	1	1 5 1
		2.6674	6	$\bar{1}$ 0 2			1.7321	3	1 2 4			1.4058	1	$\bar{3}$ 1 1
27	2.641	2.6395	15	2 1 1			1.7255	3	2 3 3	5	1.3909	1.3944	1	2 2 5
		2.6091	9	$\bar{1}$ $\bar{1}$ 2			1.7086	5	1 $\bar{1}$ 4			1.3870	3	2 5 1
		2.5811	1	2 1 0	12	1.7053	1.7009	1	3 2 2			1.3860	1	0 $\bar{3}$ 4
		2.5145	6	0 2 2			1.6996	3	$\bar{2}$ 1 2			1.3624	1	1 $\bar{4}$ 2
6	2.497	2.4922	3	2 0 1			1.6914	3	2 1 4			1.3581	1	$\bar{1}$ 5 1
		2.4545	7	2 0 0			1.6740	7	0 4 0	7	1.3552	1.3552	2	3 4 3
23	2.434	2.4332	9	$\bar{1}$ 2 0	17	1.6736	1.6694	7	2 4 1			1.3545	2	0 $\bar{4}$ 3
		2.4304	3	0 0 3			1.6657	4	1 $\bar{3}$ 2			1.3482	1	1 4 4
		2.4200	10	0 $\bar{2}$ 2			1.6647	1	1 4 2			1.3476	1	2 4 4
4	2.389	2.3932	1	2 1 2			1.6564	1	$\bar{1}$ 2 3			1.3382	1	$\bar{3}$ $\bar{3}$ 2
		2.3899	3	1 0 3			1.6540	2	2 $\bar{2}$ 2			1.3339	1	$\bar{3}$ $\bar{4}$ 1
		2.3648	2	2 2 0			1.6401	4	2 0 4			1.3329	1	$\bar{2}$ 2 3
		2.3253	1	1 3 0			1.6274	3	0 2 4			1.3263	1	4 2 1
9	2.312	2.3116	14	1 3 1	14	1.6260	1.6206	6	3 3 1			1.3197	1	4 2 2
		2.2726	3	2 0 2			1.6031	6	$\bar{1}$ 3 2			1.3136	2	4 1 1
8	2.255	2.2570	5	0 $\bar{1}$ 3			1.6011	1	$\bar{1}$ 0 4	10	1.3150	1.3104	3	$\bar{1}$ $\bar{1}$ 5
		2.2351	1	2 2 2			1.5919	3	$\bar{3}$ $\bar{1}$ 1			1.3096	1	$\bar{2}$ $\bar{5}$ 1
		2.2320	6	0 3 0			1.5901	3	$\bar{2}$ $\bar{1}$ 3			1.3082	1	0 $\bar{5}$ 1
13	2.191	2.1895	15	$\bar{2}$ 0 1			1.5892	3	3 1 3					
		2.1575	2	0 3 1			1.5820	1	$\bar{1}$ $\bar{1}$ 4					
		2.1302	3	$\bar{1}$ $\bar{3}$ 1	21	1.5882	1.5794	1	3 2 3					
		2.1262	1	1 $\bar{1}$ 3			1.5765	1	3 3 0					
		2.1101	4	$\bar{2}$ $\bar{2}$ 1			1.5731	2	$\bar{1}$ $\bar{3}$ 3					
12	2.108	2.1006	3	1 $\bar{2}$ 2			1.5698	5	$\bar{3}$ $\bar{2}$ 1					
		2.0991	10	1 3 2			1.5681	1	$\bar{2}$ 0 3					
		2.0309	1	2 3 1										

important confirmation of the presence of a hydrous component in the phase. The 2500–1200 cm^{-1} region, not shown in Fig. 5, was found to be featureless. We conclude that the H_2O bending mode, usually appearing near 1600 cm^{-1}, is either too weak to observe or is not Raman active in andychristyite.

Chemical composition

Chemical analyses (five) of andychristyite were carried out using a JEOL 8200 electron microprobe (wavelength-dispersive mode mode, 15 kV, 5 nA and 2 μm beam diameter) at the Division of Geological and Planetary Sciences, California

TABLE 2. Data collection and structure refinement details for andychristyite.

Diffractometer	Bruker D8
X-ray radiation	Mo$K\alpha$ ($\lambda = 0.71073$ Å)
Temperature	293(2) K
Structural formula	$PbCuTeO_5(H_2O)$
Space group	$P\bar{1}$
Unit-cell dimensions	$a = 5.322(3)$ Å $b = 7.098(4)$ Å $c = 7.511(4)$ Å $\alpha = 83.486(7)°$ $\beta = 76.279(5)°$ $\gamma = 70.742(5)°$
Z	2
V	260.0(2) Å^3
Density (for above formula)	6.340 g/cm^3
Absorption coefficient	41.871 mm^{-1}
F(000)	426
Crystal size (μm)	15 × 10 × 5
θ range	2.79 to 30.12°
Index ranges	$-7 \le h \le 7$, $-10 \le k \le 10$, $-10 \le l \le 10$
Reflections collected/ unique	9139/1534 [$R_{int} = 0.010$]
Reflections with $F_o > 4\sigma F$	1511
Completeness to θ = 30.12°	99.8%
Refinement method	Full-matrix least-squares on F^2
Parameters refined	98
Goof	1.077
Final R indices [$F_o > 4\sigma F$]	$R_1 = 0.0165$, $wR_2 = 0.0424$
R indices (all data)	$R_1 = 0.0168$, $wR_2 = 0.0426$
Largest diff. peak/hole	+2.97/–1.36 e^- Å^{-3}

$R_{int} = \Sigma|F_o^2 - F_o^2(\text{mean})|/\Sigma[F_o^2]$. Goof = $S = \{\Sigma[w(F_o^2 - F_c^2)^2]/(n-p)\}^{1/2}$. $R_1 = \Sigma||F_o| - |F_c||/\Sigma|F_o|$. $wR_2 = \{\Sigma[w(F_o^2 - F_c^2)^2]/\Sigma[w(F_o^2)^2]\}^{1/2}$. $w = 1/[\sigma^2(F_o^2) + (aP)^2 + bP]$ where a is 0.0288, b is 0.4223 and P is $[2F_c^2 + \text{Max}(F_o^2,0)]/3$.

Institute of Technology. The elements Se, S, Cl, Zn, Ag and Bi were sought, but not detected. The standards used were: galena (for Pb), Cu metal (for Cu) and Te metal (for Te). No other elements were detected using energy-dispersive spectroscopy analyses. There was insufficient material for CHN analyses, so H_2O was calculated on the basis of 2 (Cu + Te) and 6 O apfu, as determined by the crystal structure analysis (see below). The sample did not take a good polish and the somewhat irregular surface probably contributed to the low total. The analytical results [mean (range) (s.d.)]

TABLE 3. Fractional coordinates, occupancies and atom displacement parameters (Å^2) for andychristyite.

	x/a	y/b	z/c	U_{eq}	U^{11}	U^{22}	U^{33}	U^{23}	U^{13}	U^{12}
Pb	0.35606(3)	0.37005(2)	0.84601(2)	0.01551(6)	0.01522(8)	0.01730(8)	0.01404(8)	–0.00128(5)	–0.00487(5)	–0.00370(5)
Te	0.80489(4)	0.67520(3)	0.61955(3)	0.00815(6)	0.00873(10)	0.00819(10)	0.00778(10)	–0.00023(7)	–0.00276(7)	–0.00228(7)
Cu	0.73344(8)	0.10947(6)	0.45361(6)	0.01104(9)	0.00921(19)	0.01199(19)	0.0116(2)	0.00165(15)	–0.00370(15)	–0.00257(15)
O1	0.9216(5)	0.5510(4)	0.8339(4)	0.0136(5)	0.0139(11)	0.0168(12)	0.0081(11)	0.0001(9)	–0.0041(9)	–0.0013(9)
O2	0.1804(5)	0.5847(4)	0.4667(4)	0.0123(5)	0.0112(11)	0.0102(11)	0.0164(12)	–0.0030(9)	–0.0017(9)	–0.0045(9)
O3	0.8761(5)	0.9186(4)	0.6515(4)	0.0105(4)	0.0110(11)	0.0101(11)	0.0116(12)	–0.0002(9)	–0.0037(9)	–0.0040(9)
O4	0.4345(5)	0.7354(4)	0.7460(4)	0.0128(5)	0.0116(11)	0.0156(12)	0.0111(12)	0.0012(9)	–0.0027(9)	–0.0046(9)
O5	0.6543(5)	0.8076(4)	0.4123(3)	0.0112(4)	0.0130(11)	0.0125(11)	0.0086(11)	0.0012(9)	–0.0049(9)	–0.0036(9)
OWa*	0.168(6)	0.0864(16)	0.9663(11)	0.044(5)	0.075(13)	0.032(4)	0.022(3)	–0.001(3)	0.002(4)	–0.022(5)
OWb*	0.323(8)	0.042(4)	0.979(2)	0.041(8)	0.063(17)	0.033(8)	0.031(6)	–0.009(5)	0.012(7)	–0.030(10)
H1	0.278(11)	–0.032(7)	0.914(8)	0.050						
H2	0.189(10)	0.073(10)	0.082(3)	0.050						

*Refined occupancy of OWa = 0.63(5) and OWb = 0.37(5).

TABLE 4. Selected bond lengths (Å) in andychristyite.

Pb–O1	2.262(3)	Cu–O4	1.968(3)	Te–O1	1.883(3)
Pb–O5	2.451(3)	Cu–O3	1.991(3)	Te–O4	1.903(3)
Pb–OWb	2.473(17)	Cu–O5	1.992(3)	Te–O5	1.927(3)
Pb–O1	2.520(3)	Cu–O3	2.005(3)	Te–O3	1.938(3)
Pb–OWa	2.523(13)	Cu–O5	2.382(3)	Te–O2	1.989(3)
Pb–O4	2.754(3)	Cu–O2	2.523(3)	Te–O2	1.995(3)
Pb–O2	3.051(3)	<Cu–O>	2.144	<Te–O>	1.939
Pb–OWb	3.18(4)				
Pb–O2	3.264(3)	Hydrogen bonds			
Pb–O4	3.427(3)	OWa···O4	2.907(12)		
<Pb–O>	2.791	OWa···O3	2.822(10)		

are PbO 43.21 (42.92–43.80) (0.37), CuO 15.38 (14.98–15.64) (0.25), TeO_3 35.29 (34.95–35.64) (0.32), H_2O 3.49 (based on the structure), total 97.37 wt.%. The empirical formula (based on 6 O apfu) is $Pb_{0.98}Cu^{2+}_{0.98}Te^{6+}_{1.02}O_6H_{1.96}$. The simplified formula is $PbCu^{2+}Te^{6+}O_5(H_2O)$, which requires PbO 44.97, CuO 16.03, TeO_3 35.38, H_2O 3.63, total 100 wt.%.

X-ray crystallography and structure determination

Powder X-ray diffraction data were obtained on a Rigaku R-Axis Rapid II curved imaging plate microdiffractometer utilizing monochromatized Mo*K*α radiation. Observed powder *d*-values and intensities were derived by profile fitting using *JADE 2010* software. Data (in Å) are given in Table 1. The observed powder data fit well with those calculated from the structure, also using *JADE 2010*. The unit-cell parameters refined from the powder data using *JADE 2010* with whole-pattern fitting are: $a = 5.323(2)$, $b = 7.099(2)$, $c = 7.521(2)$ Å, $\alpha = 83.611(6)$, $\beta = 76.262(7)$, $\gamma = 70.669(8)°$ and $V = 260.34(14)$ Å^3.

Single-crystal X-ray studies were carried out using a Bruker D8 three-circle diffractometer equipped with a rotating anode generator (Mo*K*α X-radiation), multilayer optics and an APEX-II CCD area detector. Frames were measured for 90 s with a 0.3° frame width. Empirical absorption corrections (*SADABS*; Sheldrick, 2008) were applied and equivalent reflections were merged.

TABLE 5. Bond-valence sums for andychristyite. Values are expressed in valence units.

	O1	O2	O3	O4	O5	OW	Σ
Pb	0.54	0.11		0.20	0.37	0.20	2.02
	0.32	0.07		0.05		0.13	
						0.03	
Cu		0.10	0.43	0.46	0.43		1.98
			0.41		0.15		
Te	1.07	0.89	0.97	1.03	0.99		5.82
		0.88					
H1				0.14		0.86	1.00
H2			0.18			0.82	1.00
Σ	1.93	2.05	1.99	1.88	1.94	2.04	

Cu^{2+}–O bond valence parameters are from Brown and Altermatt (1985), Pb^{2+}–O are from Krivovichev and Brown (2001) and Te^{6+}–O are from Mills and Christy (2013). Hydrogen bond strengths are based on O···O bond lengths (Brown and Altermatt, 1985).

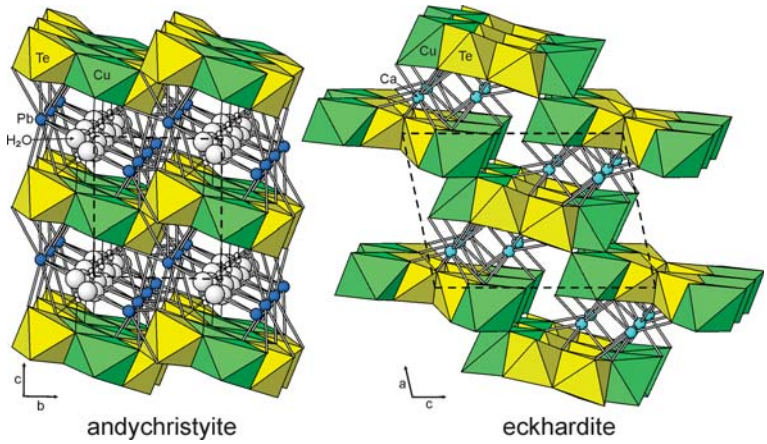

FIG. 3. The structures of andychristyite and eckhardite canted slightly along **a** and **b**, respectively. Unit-cell outlines are shown as dashed lines.

The structure was solved by direct methods using *SHELXS-2013* and the structure was refined using *SHELXL-2013* (Sheldrick, 2008). One O site, corresponding to a H_2O group, is split into two sites 0.80 Å apart (OWa and OWb). Difference-Fourier syntheses located two probable H atom positions at reasonable distances from both OWa and OWb. These H sites were refined with soft restraints of 0.90(3) Å on the O–H distances and 1.42(3) Å on the H–H distance and with the U_{eq} of each H set to 0.05. The details of the data collection and structure refinement are provided in Table 2. Fractional coordinates, occupancies and atom displacement parameters are provided in Table 3, selected interatomic distances in Table 4 and bond valences in Table 5.

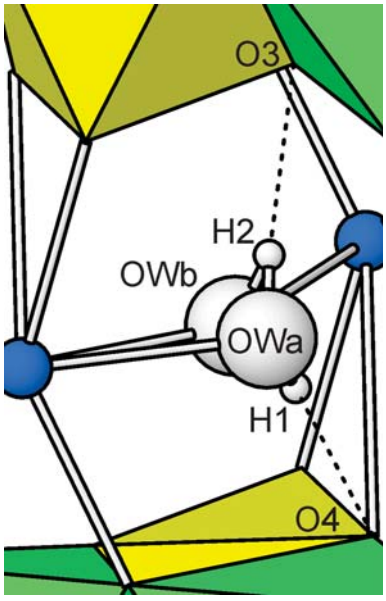

FIG. 4. Bonding of the H_2O group in andychristyite. Pb–O bonds are shown as sticks and hydrogen bonds as dashed lines. Note that the OWa site is only indicated as being bonded to one Pb site; the other Pb site shown is 3.77 Å from OWa.

Description of the structure

Andychristyite has a structure consisting of stair-step-like layers of edge-sharing $Te^{6+}O_6$ and $Cu^{2+}O_6$ octahedra parallel to {001}, which are linked in the [001] direction by bonds to interlayer Pb atoms (Fig. 3). The Pb coordination has a lopsided distribution of bond lengths to surrounding O atoms, attributable to the localization of the Pb^{2+} $6s^2$ lone-pair electrons. The split H_2O site (OWa and OWb) in the interlayer region is coordinated to Pb atoms and forms hydrogen bonds to O atoms (O3 and O4) in the layers (Fig. 4). The stair-step-like layers (Fig. 5) can be described in terms of various types of linkages between and among the regular $Te^{6+}O_6$ octahedra and Jahn-Teller distorted $Cu^{2+}O_6$ octahedra. Taken separately, the TeO_6 octahedra link by edge sharing to form Te_2O_{10} dimers and the CuO_6 octahedra link by edge sharing to form zig-zag chains parallel to [100]. Each of the 'stair-steps' is centred by a zig-zag

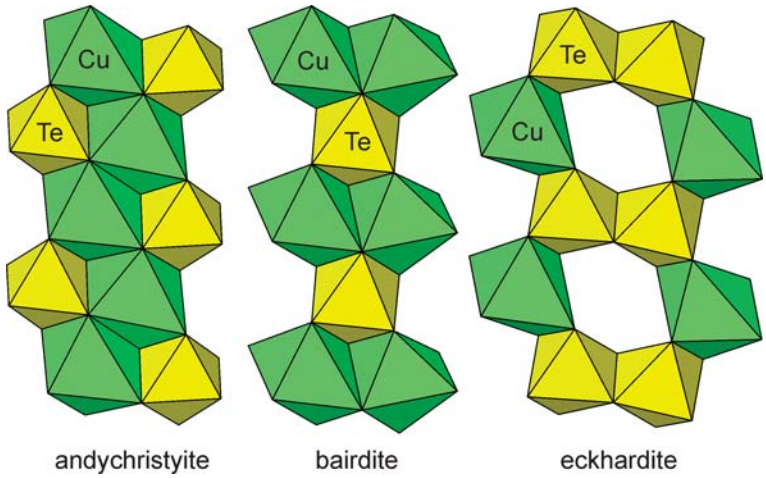

FIG. 5. The stair-step bands of octahedra in the structures of andychristyite, bairdite and eckhardite. Note that the bands in bairdite and eckhardite link to one another by sharing corners, while, the bands in andychristyite link to one another by sharing edges of the TeO_6 octahedra, forming Te_2O_{10} dimers.

chain of CuO_6 octahedra. The chains are flanked by TeO_6 octahedra on either side that share edges with the CuO_6 octahedra of the chains. The bands are linked to one another via the shared edge of the Te_2O_{10} dimers.

All minerals with known structures containing essential Te^{6+} and Cu^{2+} are listed in Table 6. All of these structures contain $Te^{6+}O_6$ octahedra and $Cu^{2+}O_6$ octahedra (or $Cu^{2+}O_5$ square pyramids). The most pertinent structural comparisons are to the minerals also containing large cations, i.e. Pb, and all such minerals, except quetzalcoatlite, are known to occur in the mineral assemblages at Otto Mountain.

An interesting feature of the stair-step-like octahedral layers in andychristyite is that they are based upon hexagonal close packing (*hcp*), not only in terms of the individual steps (or bands) of edge-sharing octahedra, but even with respect to the continuous assembly of steps. The structures of four other minerals containing Pb^{2+} (or Ca), Te^{6+} and Cu^{2+} in Table 7 are based on stair-step-like *hcp* polyhedral layers: bairdite, eckhardite, paratimroseite and timroseite. The step-forming *hcp* bands in the structures of andychristyite, bairdite, timroseite and paratimroseite are brucite-type sheet fragments, while that in eckhardite is a gibbsite-

TABLE 6. Minerals with known structures that contain both essential Te^{6+} and Cu^{2+}.

agaite	$Pb_3Cu^{2+}Te^{6+}O_5(OH)_2(CO_3)$	Kampf *et al.* (2013*b*)
andychristyite	$PbCu^{2+}Te^{6+}O_5(H_2O)$	Present study
bairdite	$Pb_2Cu^{2+}_4Te^{6+}_2O_{10}(OH)_2(SO_4)\cdot H_2O$	Kampf *et al.* (2013*c*)
eckhardite	$(Ca,Pb)Cu^{2+}Te^{6+}O_5(H_2O)$	Kampf *et al.* (2013*d*)
frankhawthorneite	$Cu^{2+}_2Te^{6+}O_4(OH)_2$	Grice and Roberts (1995)
fuettererite	$Pb_3Cu^{2+}_6Te^{6+}O_6(OH)_7Cl_5$	Kampf *et al.* (2013*a*)
housleyite	$Pb_6Cu^{2+}Te^{6+}_4O_{18}(OH)_2$	Kampf *et al.* (2010*b*)
jensenite	$Cu^{2+}_3Te^{6+}O_6\cdot H_2O$	Grice *et al.* (1996)
khinite (-4*O* and -3*T*)	$PbCu^{2+}_3Te^{6+}O_6(OH)_2$	Hawthorne *et al.* (2009)
leisingite	$Cu^{2+}_2MgTe^{6+}O_6\cdot 6H_2O$	Margison *et al.* (1997)
paratimroseite	$Pb_2Cu^{2+}_4(Te^{6+}O_6)_2(H_2O)_2$	Kampf *et al.* (2010*e*)
quetzalcoatlite	$Zn_6Cu^{2+}_3(Te^{6+}O_3)_2O_6(OH)_6(Ag_xPb_y)Cl_{x+2y}$, $x+y \leq 2$	Burns *et al.* (2000)
timroseite	$Pb_2Cu^{2+}_5(Te^{6+}O_6)_2(OH)_2$	Kampf *et al.* (2010*e*)

type sheet fragment (Fig. 5). Nevertheless, the *hcp* nature of the layers in all of these minerals is reflected in the similar cell dimensions along the lengths of the steps (andychristyite: $a = 5.322$, eckhardite: $b = 5.3076$, bairdite: $b = 5.2267$, timroseite: $a = 5.2000$ and paratimroseite: $a = 5.1943$Å).

It is noteworthy that the formulas of andychristyite and eckhardite differ only in their dominant large cation, Pb and Ca, respectively; however, as already mentioned, the octahedral layers in these structures have very different configurations. The structures of andychristyite and eckhardite are compared in Fig. 3. Besides their similar stair-step-like *hcp* polyhedral layers, these structures share another feature. Both contain edge-sharing dimers of TeO_6 octahedra $[Te_2O_{10}]$; however, the dimers play different roles. In the structure of eckhardite, both octahedra of the dimer are part of the same band, while in the structure of andychristyite, each of the two octahedra is in a different band and the shared edge of the dimer serves to link adjacent bands.

Calcium is generally rare as an essential (or even minor) component in the secondary phases at Otto Mountain. The Ca site in the structure of eckhardite contains 8.6% Pb and the site exhibits very modest asymmetry in the bond distribution. On the other hand, as noted above, the Pb site in the structure of andychristyite exhibits a marked lopsided coordination sphere, typical of Pb^{2+} with stereoactive $6s^2$ lone-pair electrons. It seems likely that the andychristyite structure preferentially incorporates Pb, while the eckhardite structure preferentially incorporates Ca, because of the abilities of the respective structures to accommodate the different stereochemistries of Ca and Pb.

The only other mineral with a structure containing an edge-sharing dimer of TeO_6 octahedra $[Te_2O_{10}]$ is thorneite, $Pb_6(Te_2O_{10})(CO_3)Cl_2(H_2O)$ (Kampf *et al.*, 2010*c*), but the structure of thorneite contains no Cu and the Te_2O_{10} dimer links only to Pb polyhedra.

Paragenesis

Andychristyite is a very rare phase, for which there are no observed contact relationships with other secondary minerals; however, considering the Te oxysalt paragenetic flowchart of Christy *et al.* (2016), we can make some predictions about its place in the Otto Mountain secondary mineral paragenesis based on its chemistry and structure. The stoichiometries of andychristyite and eckhardite are identical, except that andychristyite contains Pb instead of Ca, and the crystal structures of both contain Te as $[Te_2O_{10}]^{8-}$ dimers. Thus, we infer that it probably forms at about the same time as eckhardite, mid-to-late within the oxysalt paragenesis. Furthermore, considering that eckhardite has been reported to occur in close association with several Pb-bearing secondary phases (i.e. housleyite, khinite, markcooperite and ottoite), it is likely that the presence of Ca in the system, even if significant Pb is also present, will favour the formation of eckhardite over andychristyite.

The secondary mineral assemblages at Otto Mountain are truly remarkable for the number of new minerals that they have yielded and the fact that most of these minerals are unique to this deposit and their structures are new structure types. The presence of Pb^{2+}, Cu^{2+}, Te^{6+} and Te^{4+} in the secondary fluids is clearly important, and additional ions (i.e. Cl^-, CO_3^{2-}, SO_4^{2-}, CrO_4^{2-} and UO_2^{2+}) contribute to the diversity; however, the observation above regarding the effect of Ca^{2+} on the formation of eckhardite *vs.* andychristyite highlights the likelihood that that the absence of certain common cations (e.g. Na^+, Mg^{2+}, Ca^{2+}), at least in local microenvironments, is also critical to the formation of this remarkable mineral assemblage.

Acknowledgements

Comments by reviewers Giovanni Ferraris and Emanuela Schingaro and Structures Editor Peter Leverett are appreciated. Frank Hawthorne is thanked for providing use of the X-ray diffractometer at the University of Manitoba for collection of the structure data. The Caltech EMP analyses were supported by a grant from the Northern California Mineralogical Association and the Caltech spectroscopic work by NSF grant EAR-1322082. Part of this study has been funded by The Ian Potter Foundation grant "tracking tellurium" to SJM. The remainder of this study was funded by the John Jago Trelawney Endowment to the Mineral Sciences Department of the Natural History Museum of Los Angeles County.

References

Atencio, D., Andrade, M.B., Christy, A.G., Gieré, R. and Kartashov, P.M. (2010) The pyrochlore-supergroup minerals nomenclature. *The Canadian Mineralogist*, **48**, 673–698.

Blasse, G. and Hordijk, W. (1972) The vibrational spectrum of Ni_3TeO_6 and Mg_3TeO_6. *Journal of Solid State Chemistry*, **5**, 395–397.

Brown, I.D. and Altermatt, D. (1985) Bond-valence parameters from a systematic analysis of the inorganic crystal structure database. *Acta Crystallographica*, **B41**, 244–247.

Burns, P.C., Pluth, J.J., Smith, J.V., Eng, P., Steele, I.M. and Housley, R.M. (2000) Quetzalcoatlite: new octahedral-tetrahedral structure from $2 \times 2 \times 40$ micron crystal at the Advanced Photon Source-GSE-CARS Facility. *American Mineralogist*, **85**, 604–607.

Christy, A.G. and Grew, E.S. (2004) Synthesis of beryllian sapphirine in the system MgO-BeO-Al_2O_3-SiO_2-H_2O, and comparison with naturally occurring beryllian sapphirine and khmaralite Part 2: A chemographic study of Be content as a function of P, T and $FeMg_{-1}$ exchange. *American Mineralogist*, **89**, 327–338.

Christy, A.G. and Mills, S.J. (2013) The effect of lone-pair stereoactivity on polyhedral volume and structural flexibility: application to Te^{IV}-O octahedra. *Acta Crystallographica*, **B69**, 446–456.

Christy, A.G., Tabira, Y., Hölscher, A., Grew, E.S. and Schreyer, W. (2002) Synthesis of beryllian sapphirine in the system MgO-BeO-Al_2O_3-SiO_2-H_2O, and comparison with naturally occurring beryllian sapphirine and khmaralite Part 1: experiments, TEM and XRD. *American Mineralogist*, **87**, 1104–1112.

Christy, A.G., Mills, S.J., Kampf, A.R., Housley, R.M. Thorne, B. and Marty, J. (2016) The relationship between mineral composition, crystal structure and paragenetic sequence: the case of secondary Te mineralization at the Bird Nest drift, Otto Mountain, California, USA. *Mineralogical Magazine*, **80**, 201–310.

Frost, R.L. (2009) Tlapallite $H_6(Ca,Pb)_2(Cu,Zn)_3SO_4(TeO_3)_4TeO_6$, a multi-anion mineral: a Raman spectroscopic study. *Spectrochimica Acta Part A: Molecular and Biomolecular Spectroscopy*, **72**, 903–906.

Frost, R.L. and Keeffe, E.C. (2009) Raman spectroscopic study of kuranakhite $PbMn^{4+}Te^{6+}O_6$ – a rare tellurate mineral. *Journal of Raman Spectroscopy*, **40**, 249–252.

Grice, J.D. and Roberts, A.C. (1995) Frankhawthorneite, a unique HCP framework structure of a cupric tellurate. *The Canadian Mineralogist*, **33**, 649–653.

Grice, J.D., Groat, L.A. and Roberts, A.C. (1996) Jensenite, a cupric tellurate framework structure with two coordinations of copper. *The Canadian Mineralogist*, **34**, 55–59.

Hawthorne, F.C., Cooper, M.A. and Back, M.E. (2009) Khinite-4O [=khinite] and khinite-3T [=parakhinite]. *The Canadian Mineralogist*, **47**, 473–476.

Housley, R.M., Kampf, A.R., Mills, S.J., Marty, J. and Thorne, B. (2011) The remarkable occurrence of rare secondary tellurium minerals at Otto Mountain near Baker, California – including seven new species. *Rocks and Minerals*, **86**, 132–142.

Kampf, A.R., Housley, R.M., Mills, S.J., Marty, J. and Thorne, B. (2010*a*) Lead–tellurium oxysalts from Otto Mountain near Baker, California: I. Ottoite, Pb_2TeO_5, a new mineral with chains of tellurate octahedra. *American Mineralogist*, **95**, 1329–1336.

Kampf, A.R., Marty, J. and Thorne, B. (2010*b*) Lead–tellurium oxysalts from Otto Mountain near Baker, California: II. Housleyite, $Pb_6CuTe_4O_{18}(OH)_2$, a new mineral with Cu–Te octahedral sheets. *American Mineralogist*, **95**, 1337–1342.

Kampf, A.R., Housley, R.M. and Marty, J. (2010*c*) Lead–tellurium oxysalts from Otto Mountain near Baker, California: III. Thorneite, $Pb_6(Te_2O_{10})(CO_3)Cl_2(H_2O)$, the first mineral with edge-sharing octahedral dimers. *American Mineralogist*, **95**, 1548–1553.

Kampf, A.R., Mills, S.J., Housley, R.M., Marty, J. and Thorne, B. (2010*d*) Lead–tellurium oxysalts from Otto Mountain near Baker, California: IV. Markcooperite, $Pb_2(UO_2)Te^{6+}O_6$, the first natural uranyl tellurate. *American Mineralogist*, **95**, 1554–1559.

Kampf, A.R., Mills, S.J., Housley, R.M., Marty, J. and Thorne, B. (2010*e*) Lead–tellurium oxysalts from Otto Mountain near Baker, California: V. Timroseite, $Pb_2Cu_5^{2+}(Te^{6+}O_6)_2(OH)_2$, and paratimroseite, $Pb_2Cu_4^{2+}(Te^{6+}O_6)_2(H_2O)_2$, new minerals with edge-sharing Cu–Te octahedral chains. *American Mineralogist*, **95**, 1560–1568.

Kampf, A.R., Mills, S.J., Housley, R.M., Marty, J. and Thorne, B. (2010*f*) Lead–tellurium oxysalts from Otto Mountain near Baker, California: VI. Telluroperite, $Pb_3Te^{4+}O_4Cl_2$, the Te analogue of perite and nadorite. *American Mineralogist*, **95**, 1569–1573.

Kampf, A.R., Mills, S.J., Housley, R.M., Rumsey, M.S. and Spratt, J. (2012) Lead–tellurium oxysalts from Otto Mountain near Baker, California: VII. Chromschieffelinite, $Pb_{10}Te_6O_{20}(OH)_{14}(CrO_4)(H_2O)_5$, the chromate analogue of schieffelinite. *American Mineralogist*, **97**, 212–219.

Kampf, A.R., Mills, S.J., Housley, R.M. and Marty, J. (2013*a*) Lead–tellurium oxysalts from Otto Mountain near Baker, California: VIII. Fuettererite, $Pb_3Cu_6^{2+}Te^{6+}O_6(OH)_7Cl_5$, a new mineral with double spangolite–type sheets. *American Mineralogist*, **98**, 506–511.

Kampf, A.R., Mills, S.J., Housley, R.M. and Marty, J. (2013*b*) Lead-tellurium oxysalts from Otto Mountain near Baker, California: IX. Agaite, $Pb_3Cu^{2+}Te^{6+}O_5(OH)_2(CO_3)$, a new mineral with CuO_5–TeO_6 polyhedral sheets. *American Mineralogist*, **98**, 512–517.

Kampf, A.R., Mills, S.J., Housley, R.M., Rossman, G.R., Marty, J. and Thorne, B. (2013*c*) Lead–tellurium oxysalts from Otto Mountain near Baker, California: X. Bairdite, $Pb_2Cu_4^{2+}Te_2^{6+}O_{10}(OH)_2(SO_4)\cdot H_2O$, a new mineral with thick HCP layers. *American Mineralogist*, **98**, 1315–1321.

Kampf, A.R., Mills, S.J., Housley, R.M., Rossman, G.R., Marty, J. and Thorne, B. (2013*d*) Lead-tellurium oxysalts from Otto Mountain near Baker, California: XI. Eckhardite, $(Ca,Pb)Cu^{2+}Te^{6+}O_5(H_2O)$, a new mineral with HCP stair-step layers. *American Mineralogist*, **98**, 1617–1623.

Krivovichev, S.V. and Brown, I.D. (2001) Are the compressive effects of encapsulation an artifact of the bond valence parameters? *Zeitschrift für Kristallographie*, **216**, 245–247.

Mandarino, J.A. (2007) The Gladstone–Dale compatibility of minerals and its use in selecting mineral species for further study. *The Canadian Mineralogist*, **45**, 1307–1324.

Margison, S.M., Grice, J.D. and Groat, L.A. (1997) The crystal structure of leisingite, $(Cu,Mg,Zn)_2(Mg,Fe)Te_6{\cdot}6H_2O$. *The Canadian Mineralogist*, **35**, 759–763.

Mills, S.J. and Christy, A.G. (2013) Revised values of the bond valence parameters for Te^{IV}–O, Te^{VI}–O and Te^{IV}–Cl. *Acta Crystallographica*, **B69**, 145–149.

Mills, S.J., Christy, A.G., Kameda, T., Génin, J.-M.R. and Colombo, F. (2012) Nomenclature of the hydrotalcite supergroup: natural layered double hydroxides. *Mineralogical Magazine*, **76**, 1289–1336.

Mills, S.J., Kampf, A.R., Christy, A.G., Housley, R.M., Rossman, G.R., Reynolds, R.E. and Marty, J. (2014) Bluebellite and mojaveite, two new minerals from the central Mojave Desert, California, USA. *Mineralogical Magazine*, **78**, 1325–1340.

Sheldrick, G.M. (2008) A short history of SHELX. *Acta Crystallographica*, **A64**, 112–122.